# Open-source approach for reproducible substrate mapping using semantic segmentation on recreation-grade side scan sonar datasets

Cameron S. Bodine[a,*], Daniel Buscombe[a,b], Toby D. Hocking[a]

[a]*Northern Arizona University School of Informatics, Computing, and Cyber Systems, Building 90, 1295 S. Knoles Dr., Flagstaff, AZ, 86011, United States of America*

[b]*Northern Arizona University School of Earth and Sustainability, Room A108 Building 11, 624 S. Knoles Dr., Flagstaff, AZ, 86011, United States of America*

**Abstract**

Knowledge of the variation and distribution of substrates at large spatial extents in aquatic systems, particularly rivers, is severely lacking, impeding species conservation and ecosystem restoration efforts. Air and space-borne remote sensing important for terrestrial and atmospheric measurements are limited in benthic environments due to river stage, turbidity, and canopy cover, requiring direct observation of conditions in the field. Recreation-grade side scan sonar (SSS) instruments, or fishfinders, have demonstrated their unparalleled value as a low-cost scientific instrument capable of rapidly imaging benthic environments due to the ease of deploying and operating the instrument. However, existing methods for generating georeferenced datasets from these instruments, including sonar mosaics and substrate maps, remains a barrier of adoption for wider scientific inquiry due to the high degree of

*Corresponding author.

*Email address:* csb67@nau.edu (Cameron S. Bodine)

human-intervention and expertise required to generate these datasets. To address this short-coming, we introduced PING-Mapper; an open-source and freely available Python-based software for generating geospatial benthic datasets from popular Humminbird® instruments reproducibly, with minimal intervention from the user. The previously released Version 1.0 of the software provided automated workflows for exporting georeferenced sonar imagery. This study extends functionality with Version 2.0 by incorporating semantic segmentation with deep neural network models to reproducibly map substrates at large spatial extents. We present a novel approach for generating label-ready sonar datasets, creating label-image training sets, and model training with transfer learning; all with readily available open-source tools. The substrate models, achieving overall accuracies of 78%, are integrated into PING-Mapper v2.0, providing an automated workflow to generate map substrate distribution anywhere. Additional workflows enable masking sonar shadows, calculating independent bedpicks, and correcting attenuation effects in the imagery to improve interpretability. This software provides an improved mechanism for generating geospatial benthic datasets from recreation-grade SSS systems, thereby lowering the barrier for inclusion in wider aquatic research.

*Keywords:*

Side-scan sonar, Substrate mapping, Aquatic habitat, Acoustical remote sensing, Deep learning, Semantic segmentation

---

## 1. Introduction

Surveying and mapping approaches for aquatic systems, particularly riverscapes, have been increasingly investigated due to a recognized need for a holistic perspective of these ecosystems (Torgersen et al., 2022). Traditional point and transect based approaches are spatiotemporally limited and require model-based approaches to interpolate between study sites (Peterson et al., 2013; Brennan et al., 2016), resulting in smoothed depictions of aquatic characteristics which fail to capture the nuance high-resolution datasets provide (Carbonneau et al., 2012). High-resolution air- and space-based remote sensing approaches have shown beneficial in locating sediment bars with satellite imagery (Carbonneau and Bizzi, 2023) and imaging substrate from Unmanned aerial vehicles (UAVs) (Myrvold and Kind Dervo, 2020). However, these approaches require ideal conditions such as limited cloud cover at baseflow or low altitude with transparent water, which limits their applicability to all rivers due to highly dynamic conditions and settings.

Vessel-mounted sonar instruments, particularly side-scan sonar (SSS) (Chesterman et al., 1958; Klein and Edgerton, 1968; Singh et al., 2000; Brown et al., 2011), are a technology which effectively image large swaths (e.g., up to $\approx$ 90 m total width at 455kHz (Kaeser et al., 2013)) of the benthos at high resolutions. This technology was previously only available as sophisticated survey-grade sonar systems, requiring large project budgets and extensive technical expertise to operate. However, recreation-grade fishfinders, introduced in 2005 (Humminbird® 981c), were quickly repurposed as scientific instruments (Kaeser and Litts, 2008, 2010). This enabled high-resolution surveys across the landscape (Kaeser et al., 2013) and a democratization of

aquatic surveys with acoustics (Buscombe, 2017). While these systems lack many of the features and positional accuracies of their survey-grade counterparts, they nevertheless have proven an effective tool for efficient imaging of shallow aquatic systems at large spatial extents.

Recreation-grade SSS instruments have enabled scientists to manually and semi-manually map the benthos. Applications include mapping large wood (Kaeser and Litts, 2008; Holcomb et al., 2020), substrate (Kaeser and Litts, 2010; Kaeser et al., 2013; Cheek et al., 2016; Walker and Alford, 2016; Scholl et al., 2021), meso-habitats (Smit and Kaeser, 2016; Kaeser et al., 2019), fish abundance (Bollinger and Kline, 2017; Lawson et al., 2020; Wolfenkoehler et al., 2023), and aquatic vegetation (Bennett et al., 2020). These rich datasets come at a high cost, however. The highly specialized task of delineating and classifying features from sonar mosaics, particularly substrate, largely remains a manual and time-consuming task undertaken by a human, making these approaches prone to mapping variability and classification errors at large spatial extents. An accurate, fast, reproducible, and automated approach for substrate mapping is the next phase in repurposing recreation-grade SSS systems for mapping aquatic environments.

There has been an increase in automated approaches to classifying SSS datasets in recent years, showing potential for efficient and reproducible benthic mapping. Unsupervised approaches to calculating texture metrics from the imagery have been made available in open-source toolsets (Buscombe et al., 2016; Buscombe, 2017; Hamill et al., 2018), however it is unclear how texture relates to substrate. Supervised approaches, particularly deep learning for semantic segmentation, have recently been used to characterize SSS

datasets collected with survey-grade and recreation-grade sonar instruments (Steiniger et al., 2022). Deep learning based approaches have included segmenting the water column (Zheng et al., 2021), prominent lines (Wu et al., 2019; Wang et al., 2020), discriminating objects from sonar shadows and background (Song et al., 2021), sand waves (Yu et al., 2019; Li et al., 2019; Nian et al., 2021), and seagrass and potholes (Rahnemoonfar and Dobbs, 2019). However, only four of these studies are focused on benthic habitat and primarily consider binary classifications, limiting their application to heterogeneous habitats. Additionally, the models and datasets are not open-source, impeding community-driven application and refinement of these approaches.

The first step towards efficient reproducibility came with the release of PING-Mapper v1.0 (Bodine et al., 2022; Bodine and Buscombe, 2022), an open-source software which transforms sonar recordings collected with Humminbird® side imaging systems into georefrenced datasets with minimal intervention from the user. It is compatible with any existing Humminbird® model and exports geometrically corrected sonar image mosaics that can be viewed and analyzed in any geographic information system (GIS) software. In this study, we present a new release of PING-Mapper v2.0 (Bodine and Buscombe, 2023a) which incorporates deep neural network models that automatically locate and mask sonar shadows, calculate independent bedpicks from both side-scan channels, and classify substrates at the pixel level. We will discuss the method for generating label-ready sonar images, the creation of pixel-wise substrate labels, model training, model evaluation, creation of substrate maps from model predictions, and opportunities for improvement.

## 2. Materials and methods

Sonogram visual interpretation and manual mapping is the state-of-the-art for mapping substrates in aquatic systems (Kaeser and Litts, 2010; Kaeser et al., 2013), however these methods are tedious and not reproducible (Buscombe et al., 2016). The primary objective of this study is to train deep learning models for automated and reproducible semantic segmentation of substrates and bedforms visible in side-scan sonar imagery. In semantic segmentation, pixel-wise labels, encoded as integers, are predicted from image pixel values (Buscombe and Goldstein, 2022). These models require many image-label pairs to train. Open-source datasets of SSS imagery and substrate labels are not available (Steiniger et al., 2022), therefore this study first created the datasets using open-source software (i.e., PING-Mapper (Bodine and Buscombe, 2022), Doodler (Buscombe et al., 2022), and Make Sense (Skalski, 2019)) from recreation-grade sonar datasets collected on the Pearl and Pascagoula river systems in Mississippi. Segmentation models were then fit to the datasets with Segmentation Gym (Buscombe and Goldstein, 2022). Finally, automated mapping routines were added to PING-Mapper v2.0 (Bodine and Buscombe, 2023a), providing an efficient and reproducible substrate mapping workflow requiring minimal human-interaction. The following sections provide additional detail.

### *2.1. Side-scan sonar overview*

Side-scan sonar is an acoustic technology used to image benthic environments. A pole-mounted transducer fixed to the bow (Kaeser et al., 2013) or attached to a towfish emits a high-frequency (approx. 400-1,200 kHz) pulse,

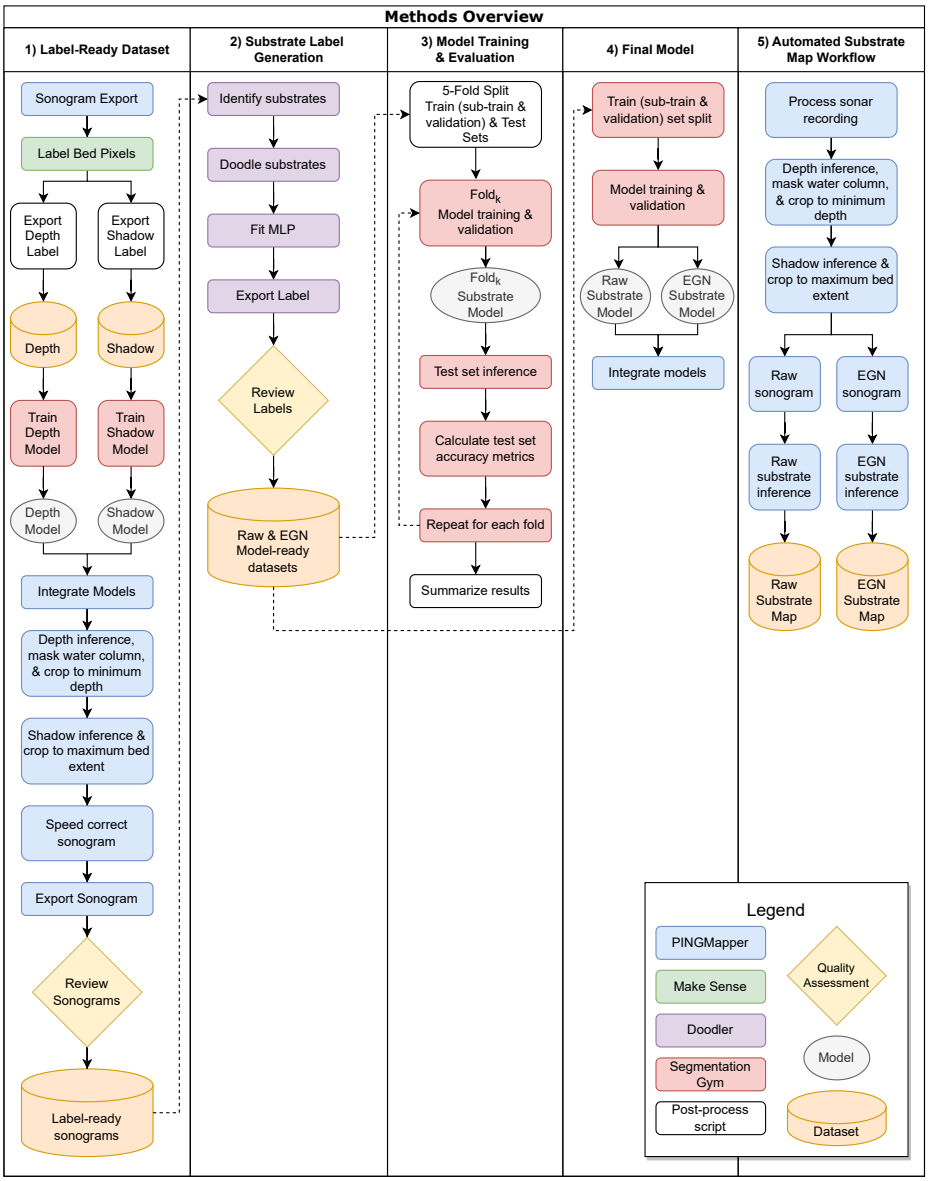


Figure 1: Methods overview diagram for 1) creating label-ready dataset; 2) creating the substrate labels; 3) substrate model training and evaluation; 4) final model training; and 5) integrating the automated substrate mapping workflow in PING-Mapper. The color of the rectangular boxes indicate the open-source method used, the diamonds indicate where data quality were qualitatively checked, the gray ovals indicate the trained models, and the orange cylinders show the datasets generated from this study.

or ping, to the port and starboard side of a moving vessel (see Figure 1 in Buscombe (2017)). As the vessel moves, sound pulses are repeatedly generated and returns from the bed, or backscatter, are recorded (Blondel, 2009). Humminbird® side-scan systems convert the backscatter to 8-bit unsigned integers [0-255]. Stacking the integers in a time series results in an image showing the water column at nadir, bed, and acoustic shadows. This image is referred to here as a sonogram. With the position information measured by an internal or external GPS and assumptions concerning the sonar beam pattern (Buscombe, 2017), the sonogram can be warped to the vessel track, resulting in a georectified mosaic of the aquatic system (Bodine et al., 2022).

### *2.2. Data collection*

Sonar surveys were conducted on rivers in the Pearl and Pascagoula watersheds in Mississippi, USA (Figure 2) by staff from the University of Mississippi (USM) Estuarine and Movement Ecology Lab (EMEL) and the U.S. Fish and Wildlife Service (USFWS) Panama City, FL. Survey data were collected with four Humminbird® Solix 12 Chirp Mega SI+ G2 during periods of high discharge, typically late winter and spring months, in 2021-2023. An operating frequency of 1,200 kHz was used, except in rare cases when water conditions were not appropriate (i.e., high turbidity or aeration), in which case the frequency was switched to 455 kHz. A summary of the data collected is presented in Table 1.

### *2.3. Image-label dataset creation*

The following sections detail the creation of image-label datasets used to train, validate, and test semantic segmentation models.

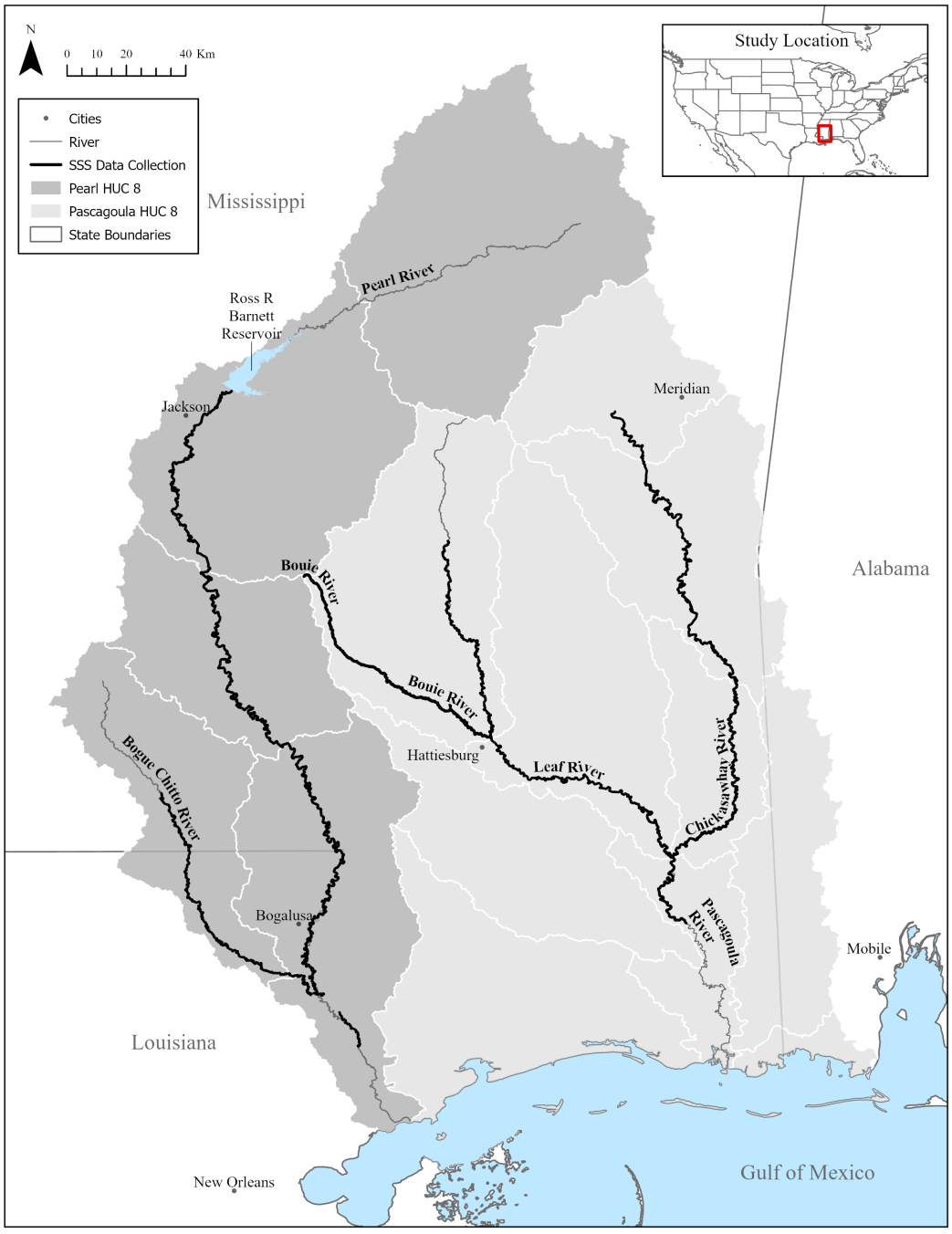


Figure 2: Coverage of side-scan sonar data collected on the Pearl and Pascagoula watersheds in Mississippi, USA.

| River | Field Days | Duration [hh:mm] | Distance [km] | Sonar Return Count | Avg. Speed [km/h] | Avg. Range [m] | Avg. Depth [m] |
|---|---|---|---|---|---|---|---|
| Pearl | 14 | 84:29 | 853.2 | $1.69 \times 10^{10}$ | 10.2 | 33.6 | 4.1 |
| Bogue Chitto | 7 | 17:13 | 153.4 | $2.63 \times 10^{8}$ | 9.0 | 28.1 | 2.0 |
| Pascagoula | 2 | 08:18 | 81.4 | $1.50 \times 10^{9}$ | 9.8 | 42.8 | 3.0 |
| Leaf | 7 | 29:01 | 268.3 | $4.81 \times 10^{9}$ | 9.3 | 34.1 | 2.4 |
| Bouie | 2 | 03:40 | 32.7 | $5.35 \times 10^{8}$ | 9.0 | 25.6 | 2.4 |
| Chickasawhay | 4 | 27:19 | 259.8 | $4.87 \times 10^{9}$ | 9.5 | 40.6 | 4.2 |
| Chunky | 3 | 02:48 | 28.6 | $4.05 \times 10^{8}$ | 10.5 | 27.1 | 3.9 |
| Total/Avg. | 38 | 132 | 172:18 | 1674.5 | 9.8 | 34.5 | 3.6 |

Table 1: Summary of sonar surveys conducted in the Pearl and Pascagoula watersheds in Mississippi, USA. Note that the range (per-side) is reported rather than the swath (total width).

#### *2.3.1. Dataset masking and cropping*

Prior to creating the substrate dataset, two filtering steps were undertaken to speed and simplify label generation on a subset of the available sonograms: 1) masking water column and cropping to minimum depth, and 2) locating sonar shadow regions caused by the river bank and cropping the sonogram to the maximum extent of the bed. Raw SSS sonograms have returns, or pixels, from three main sources: 1) the water column at nadir; 2) substrates and objects on the bed; and 3) shadows caused by objects, bedforms, and from the river bank. The sonar recordings used in this study are from dynamic river environments which have highly variable depths and widths (Table 1). These factors influence high variation in the quality of the sonograms, including the proportion of pixels from the bed compared to those

from the water column and shadows. Therefore, sonograms were masked and cropped to maximize the proportion of bed pixels in the sonogram.

The depth measured by the sonar sensor is typically used to locate the water-bed interface and remove water column pixels (Cobra et al., 1992), however, these depth estimates are prone to errors (Zheng et al., 2021). Additionally, there is no information available on the sonar system to locate and mask shadows. Therefore, masks were manually created. First, sonar recordings from the Pearl, Bogue Chitto, Leaf, Bouie, and Chickesawahay were processed with PING-Mapper (Bodine and Buscombe, 2022) and sonogram tiles (500 pings x sonar range) with the water column present (WCP) were exported. Port and starboard sonogram pairs were randomly sub-sampled, resulting in 2,000 sonograms for labeling. Make Sense (Skalski, 2019), an open-source browser-based software, was used for generating vector labels for the sonograms (Figure 3). A single polygon was delineated around the pixels from the bed, leaving the water column (top) and shadows caused by the river bank (bottom) un-labeled. Pixel indices of the polygon coordinates were exported to JSON (JavaScript Object Notation) files. Scripts were written to convert the polygon into binary labels, classified as water column or shadows (0), and bed (1). Depth and shadow models (see Section 2.4.1) where trained using the water column and shadow labels, respectively.

### *2.3.2. Label-ready sonograms*

Workflows were added to PING-Mapper to export label-ready sonograms used for annotating the substrate labels. PING-Mapper processes sonar recordings based on a user-provided chunk size which indicates the batch size, or number of pings, which will be loaded into memory at once (Bodine

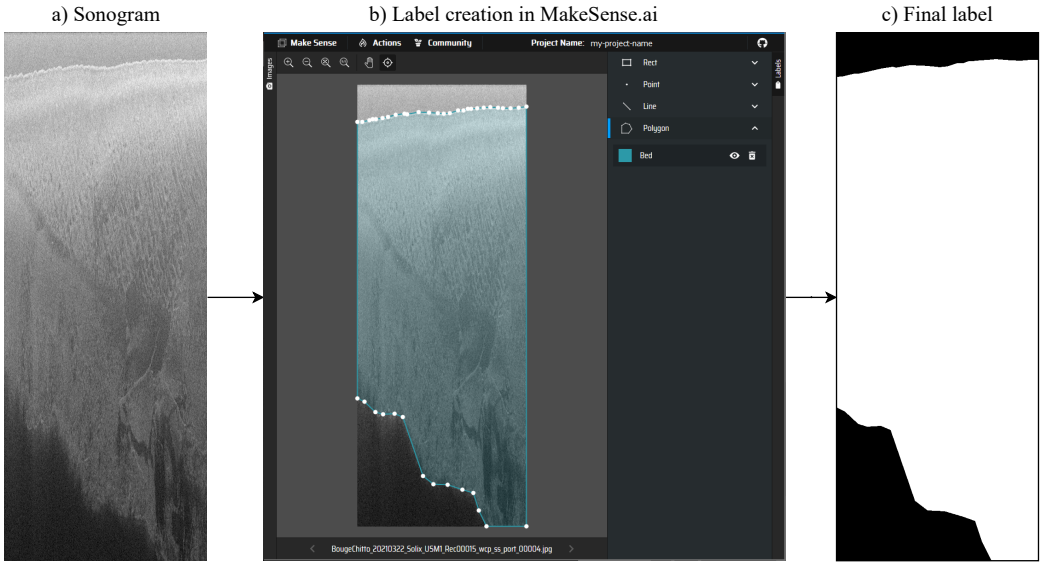


Figure 3: Depth and shadow label generation with MakeSense.ai. Panel a shows the raw sonogram (height = range setting, 1308 pixels; width = 500 pixels), panel b shows the delineation of a polygon around non-water column pixels, and panel c shows the final label after conversion to raster where the black pixels at the top are water column labels, white are bed labels, and black at the bottom are shadow labels.

et al., 2022). A default of 500 pings was used, which is the width, in pixels, of the sonogram shown in panel a of Figure 3. The range, or height of the sonogram in pixels, depends on the range set during the survey and is therefore variable. For each chunk, PING-Mapper uses the depth model to predict the depth of each ping in the sonogram. Water column pixels are masked using the depth predictions, and the top of the sonogram is cropped to the minimum depth. Second, shadows are predicted using the shadow model. Shadow patches which touch the far range are used to locate the farthest return from the bed, and the bottom of the sonogram is cropped to this range. This process speeds up substrate labeling by reducing the number of classes and pixels to annotate by removing non-substrate (i.e., water column, shadow) pixels through masking and cropping. The width of the sonograms is compressed compared to the height because the width does not account for distance traveled by the vessel. Therefore, in the final processing step, the width of each chunk is rescaled by the along-track distance covered by the vessel, resulting in an aspect ratio which is more representative of the distances the width and height cover. This step aids the interpretation of the sonogram, allowing refined annotation of small substrate patches. For reference, a speed-corrected sonogram is shown in Figure 5.

Label-ready sonograms from the port and starboard channels were exported from all available sonar recordings, totaling ∼30,800 files. The sonograms were visually reviewed and those which had inaccurate water column removal or cropping were removed from consideration. The remaining files were assessed as to the type and variety of substrates present. A total of ∼3,700 files were selected for substrate labeling.

*2.3.3. Substrate identification*

Gulf coastal plain rivers are typically dominated by sand, particularly in lower reaches, while rocky substrates are generally isolated to upper extents (Ward et al., 2005). This study sought to distinguish fine substrates (i.e., sand, silt, and mud) from rocky substrates (i.e., gravel, cobble, boulder, bedrock). Visual identification of substrates from sonograms is a non-trivial process requiring experience and field validation. Sonar intensity, texture, and context are taken into account during interpretation to identify homogeneous patches with uniform signatures indicating different substrate types (Kaeser et al., 2013). Several examples are shown in Figure 4). Fine substrates (i.e., sand) form rippled and duned bedforms casting shadows and tone variations. Coarse fine substrates (i.e., gravel, small cobble) form homogeneous, smooth bedforms, bright image tones, and are located on point-bars, deep pools, and adjacent to patches of rocky substrates. Rocky substrates (i.e., large cobble, boulder) are large enough to resolve individual objects owing to the sonar shadows they cast. Hard bottom substrates (i.e., bedrock, consolidated clay) have highly variable textures and edges with variable pixel intensities.

The Bouie, Leaf, and Chunky rivers were visited in September 2022 to validate sonar interpretation. Prior to the field visit, sonar mosaics were processed with PING-Mapper and loaded into geographic information system (GIS) software. Mosaics were visually examined in conjunction with field photos, notes and satellite imagery. Gravel, cobble, boulder, hard bottom, or uncertain substrate patches were flagged with a point or polygon. Flagged locations and sonar mosaics were loaded onto a tablet and were visited in the

field. Substrates were examined by diving, prodding with a pole, or touch and compared with the sonar mosaic. Notes on substrate classification, context, adjacent substrate and photos were taken at each location. This information provided confirmation that gravel (Figures 4a-4b), cobble/boulder (Figures 4c-4d), and hard bottom (Figures 4e-4f) could be reliably interpreted in most situations. Once substrates were reliably identified, substrate labels were generated.

*2.3.4. Substrate labeling*

Doodler (Buscombe et al., 2022) is an open-source interface for quickly generating labels from sparse annotations provided by a human. The human annotates pixels belonging to classes of interest, provided in an auxilary file, in a browser-based graphical user interface (GUI). For each image, the associated doodles are used to fit a Multi-Layer Perceptron (MLP) (Bishop, 2006) model, resulting in pixel-wise probabilistic classification, and additionally refined with a fully connected conditional random field (CRF) (Kumar and Hebert, 2006). For each label-ready sonogram, homogeneous patches of sonar pixels belonging to substrate classes of interest (Table 2) were visually identified and manually annotated with the corresponding substrate class, resulting in pixel-wise substrate label for all the label-ready sonograms (see 2.3.2). An example of a label-ready sonogram, Doodles, and final label are shown in Figure 5. All labels were annotated by C.S. Bodine who has over 5 years of experience of visually identifying substrates from recreation-grade sonar imagery, manually delineating and mapping substrate boundaries, and validating substrate maps in the field. A final visual quality assessment of the labeled sonograms identified labels which were unintentionally misclassi-

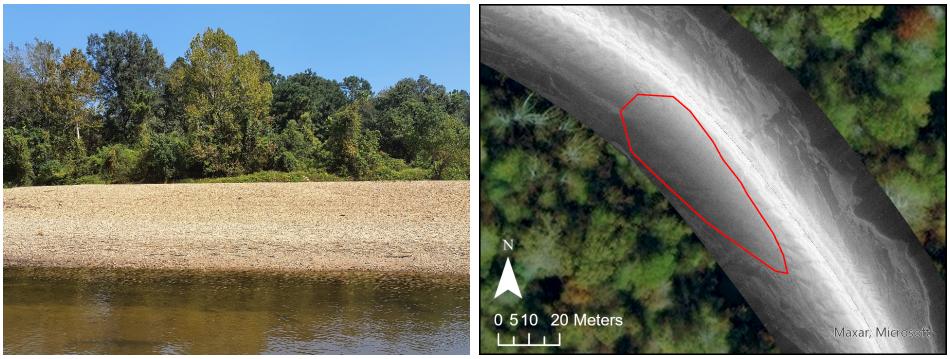

(a) Gravel.




(b) Sonar mosaic of gravel.

(c) Cobble and boulder.

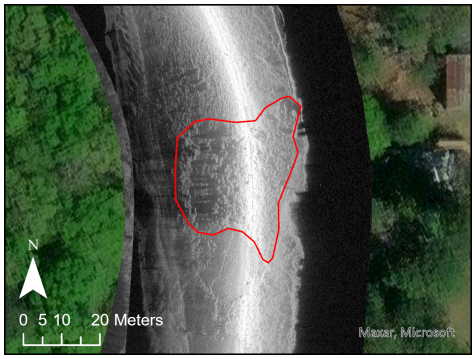


(d) Sonar mosaic of cobble and boulder.

(e) Bedrock shelf with boulders.

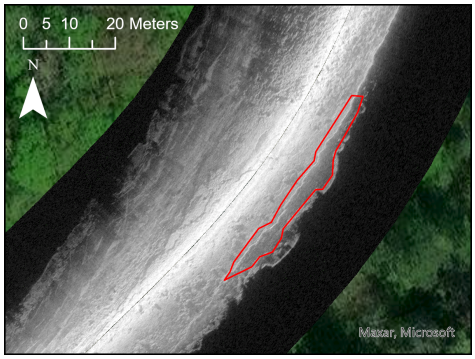


(f) Sonar mosaic of bedrock shelf with boulders.

Figure 4: Field photos and sonar mosaic of gravel 4a-4b, cobble-boulder 4c-4d, and bedrock 4e-4f.

| Class | Substrate | Description |
|---|---|---|
| Fines - Rippled | Sand | Sonogram patches with clearly visible ripples. |
| Fines - Flat | Gravel, potentially sand, silt or mud | Sonogram patches with smooth bedform and homogeneous texture. |
| Cobble / Boulder | Cobble and boulder chunks composed of rock, bank material, or hard clay | Sonogram patches with discernible objects which cast shadows. |
| Hard bottom | Hard clay and bedrock | Sonogram patches with variable textures, edges, and sonar intensities. |
| Wood | Large tree trunks and branches | Sonogram patches with linear, branching features with shadows. |
| Other | Unsure, cultural, etc. | Sonogram patches where substrate cannot be inferred, or are constructed such as bridge pilings. |

Table 2: Substrate classification scheme for sonogram label generation and modeling.

fied, or those which the Doodler model output failed to accurately capture substrate patches. The final training set consists of ∼2,750 sonogram and label pairs (Bodine, 2023). Of the $3.16 \times 10^{10}$ sonar returns in the entire dataset (see Table 1), a total of $5.30 \times 10^{8}$ (1.7%) of the dataset was labeled, which is ∼2.2 km$^2$ instream area.

### *2.4. Model training*

In supervised machine and deep learning, models are trained on datasets in order to learn a function $f(x) = y$ where $x$ is a set of inputs, or features, and $y$ is the output, or label (Murphy, 2012). The datasets are randomly

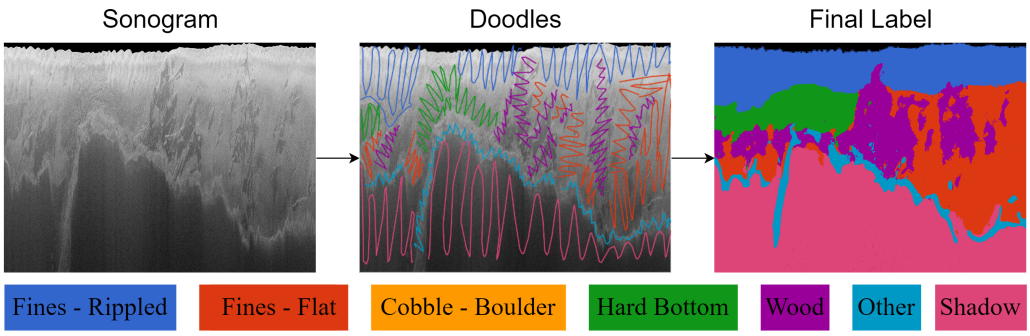


Figure 5: Substrate label generation process. The raw sonogram is loaded into Doodler, classes are visually interpreted and annotated with doodles, and the doodles are used to train a model to segment the remaining pixels.

split into a training and test set. The training set is subset into train and validation subsets. Over a series iterations, or epochs, the images in the train subset are passed to the model which learns to map the inputs to the outputs. Learned parameters, or weights, are updated by optimizing the distribution of accuracy metrics on the validation set (i.e., calculating pixel-wise agreement between the model prediction and label) through the use of a loss function. To avoid over-fitting and ensure the model will generalize well to new datasets, predictions are made on the images in the validation set and compared to their labels which are used to update various hyper-parameters including learning rate.

Segmentation Gym is a pipeline for quickly prototyping segmentation models for the geosciences (Buscombe and Goldstein, 2022). A menu of model architectures are available, including tunable hyper-parameters specified in a configuration file. A script to generate model-ready datasets is provided to transform image and label pairs into a structure the software

expects by; a) standardizing the imagery, b) resizing the files to a common target size, c) sub-setting the datasets into train and validation sets, and d) undergoing a series of augmentation steps to transform the data (flipping, rotating, shifting, etc.). Only the train subset underwent data augmentation to ensure there was no leak of validation data into the train set. Once the model-ready datasets are generated, they are passed to Segmentation Gym to train the models. Segmentation Gym utilizes a varying learning rate set deterministically as a function of training epoch, with minimum and maximum specified as a hyper-parameter. The learning rate is initially set at the minimum, quickly increases to the maximum, then decays exponentially, allowing slow convergence to an optimum (see Buscombe and Goldstein (2022) for detailed explanation). The following subsections provide additional detail.

### *2.4.1. Depth and shadow models*

This study is focused on predicting and mapping substrate, therefore pixels belonging to non-substrate pixels, such as the water column at nadir and sonar shadows, are masked to ensure they are not mistakenly misclassified as a substrate. Depth and shadow models were trained with the image-label dataset masks (Section 2.3.1) to automatically segment and mask the water column and sonar shadows.

The depth modeling workflow follows several procedures outlined in (Zheng et al., 2021). First, the port and starboard scans are merged into 500 ping sonograms. The merged sonograms were converted into a three-band image by stacking the mirrored image and the average of the original and mirrored image. The three-band sonogram was then randomly cropped, up to the

maximum depth, to create datasets with varying proportion of pixels belonging to the water column. This increases the total number of datasets used for training and produces images closer to the target size used for training (512 x 512 pixels), ensuring accurate bedpicks. The image-label pairs were converted to model-ready datasets using utilities available in Segmentation Gym. A series of width and height shifts were made to further augment the imagery. A total of ∼6,500 datasets were created for model training and validation.

The depth model was trained with a Residual UNet architecture. The UNet (Ronneberger et al., 2015) is a fully convolutional (no fully connected layers) architecture which utilizes four convolutional "blocks" made up of convolutional and batch normalization layers, connected by ReLu activations with the option to add dropout layers. The Residual UNet adds residual connections (Drozdzal et al., 2016) which aid information flow (Zhang et al., 2018; Liu et al., 2019; Nagi et al., 2021). Hyperparameters were set based on previous experience including a kernal size of 3, stride of 2, 8 filters per convolutional block, no dropout, categorical cross-entropy loss function, a varying learning rate of $1e^{-7} - 1e^{-4}$ (Buscombe and Goldstein, 2022). The model was fit over 35 epochs, with an early stopping criteria of 10 epochs specified to avoid overfitting. The model achieved a train and validation loss of 0.01 and 0.02, respctively, and train and validation mean IoU (see Section 3 for more information) of 0.99 and 0.98, respectively.

Model-ready datasets for the shadow model were created by first masking the water column with the depth mask and cropping to the minimum depth. This ensures water column pixels are not mistakenly classified as shadow.

A total of ∼3,100 datasets were made after applying height and width shift and horizontal flip augmentation. A Residual UNet model was trained with a kernel size of 9, stride of 2, 6 filters per convolutional block, dropout of 0.1, dice loss function, and varying learning rate of $1e^{-7} - 1e^{-4}$ (Buscombe and Goldstein, 2022). The model was fit over 59 epochs, with an early stopping criteria of 10 epochs specified to avoid overfitting. The model achieved a train and validation loss of 0.02 and 0.03, respectively, and train and validation mean IoU of 0.93 and 0.88, respectively.

*2.4.2. Substrate model*

Substrate models are trained using both raw and EGN sonograms (see Section 2.5). Substrate labels were first made using the raw sonograms, as outlined in Section 2.3. A new set of EGN sonograms were exported and aligned to the existing substrate labels. This allows investigation of the impact of normalizing on model predictions. The sonogram-label dataset is class imbalanced (Fines Ripple: 38.0%; Hard Bottom: 25.3%; Fines Flat: 24.8%; Cobble Boulder: 4.4%; Other: 3.8%; Wood: 3.6%), therefore a stratified sample based on proportion of each substrate present in a given label so that each class is represented in the train, validation, and test subset (Kubat, 2017). Through hashing, a strataID was assigned to each label, and coded based on the proportion of each class: 'L' < 10%; 10% < 'M' <= 50%; and 'H' > 50%. To limit the total unique combinations, only Fines - Rippled, Fines - Flat, and Wood were coded individually. Cobble / Boulder and Hard bottom were combined and coded. The strataID also indicated which river the sample was from, as the datasets represent 7 different rivers in two watersheds in Mississippi (Bouie: 49.5%; Leaf: 40.2%; Pearl: 6.4%; Bogue Chitto:

1.9%; Chickasawhay: 1.6%; Chunky: 0.4%).

The substrate model utilized the pre-trained SegFormer architecture (Xie et al., 2021). SegFormer architecture consists of a Transformer encoder to extract image features which are passed through a fully connected multilayer perceptron. The implementation of SegFormer in Segmentation Gym utilize the model architecture and pre-trained weights of the Xie et al. (2021) model instance, which were originally fine-tuned on the large ADE20k dataset (Zhou et al., 2019) at a resolution of 512x512 pixels. Through 'transfer learning' (Niu et al., 2020), the model originally trained for one segmentation task was fine-tuned on the current task of segmenting substrates from sonograms. A varying learning rate of $1e^{-8} - 1e^{-5}$ was used as a faster learning rate did not minimize train and validation loss. Two five-fold cross-validation experiments, discussed in Section 3, were used to assess model performance and ensure that random train, validation, and test splits had no effect on model performance. Following evaluation of the experiment, final Raw and EGN models were fit using all available datasets without a hold-out test set. The final Raw model was fit over 67 epochs, with an early stopping criteria of 10 epochs specified to avoid overfitting. The Raw model achieved a train and validation loss of 0.47 and 0.43, respectively, and train and validation mean IoU of 0.86 and 0.83, respectively. The final EGN model was fit over 100 epochs and stopped as specified by the maximum number of allowed epochs. The EGN model achieved a train and validation loss of 0.47 and 0.48, respectively, and train and validation mean IoU of 0.85 and 0.82, respectively.

*2.5. Empirical Gain Normalization*

Sonogram image quality degrades due to attenuation (loss of signal over distance) and water conditions (turbidity, oxygenation, temperature, etc.). This results in higher backscatter near nadir which degrades with increasing range. Therefore, an approach for normalizing the imagery based on range and incidence angle called Empirical Gain Normalization (Chesapeake Technology Inc., 2023) was adapted and integrated into PING-Mapper. The documentation (Chesapeake Technology Inc., 2023) lacked a formal definition of the normalization procedure, therefore, it is described in detail here.

Ping returns, or acoustic backscatter intensity values, are stored in 8-bit [0-255] encoding, $b(x, y)$, where $x$ and $y$ are part of a rectangular coordinate system, creating a monochrome 2D image, $S[m, n]$ where $m = 1...M$ and $n = 1...N$ are image coordinates, with $m$ representing the spanwise (horizontal) coordinate and $n$ representing the along-track vessel coordinate. Therefore (Cobra et al., 1992; Buscombe, 2017),

$$S[m, n] = b(x, y)|_{\substack{x=x_s[m,n], \\ y=y_s[m,n]}} \tag{1}$$

Geometric corrections known as slant-range correction (Cobra et al., 1992) are first applied to the backscatter. The height of the water column at nadir, available in the sonar recording or automatically estimated (see Section 2.4.1), is used to convert the slant-range to a planer range, assuming a flat-bottom due to unknown depths across the swath. Taking the original sonogram with the water column present, $\bar{S}[l, n]$, and the height of the water column, $h[n]$, the slant-range is converted to a planer range. Therefore (Cobra et al., 1992),

$$S[m,n] = \bar{S}[l,n]|_{l=\sqrt{h^2[n]+m^2}} \tag{2}$$

for $m = 1...M$ and $n = 1...N$ as described previously, and gaps in the data following redistribution are filled via interpolation (Bodine and Buscombe, 2022). The global mean of the backscatter, $\boldsymbol{A}[m]$, along the vessel track $n$, is calculated for each spanwise pixel $m$, resulting in a vector of means $\boldsymbol{A}$. Therefore,

$$\boldsymbol{A}[m] = \frac{1}{N}\sum_{n=1}^{N} S[m,n] \tag{3}$$

The backscatter values in $S[m,n]$ are subsequently normalized by dividing each $n$-wise vector by $\boldsymbol{A}$, resulting in a normalized matrix denoted $\hat{S}[m,n]$ where $m = 1...M$ and $n = 1...N$. Therefore,

$$\hat{S}[m,n] = \frac{S[m,n]}{\boldsymbol{A}[m]} \tag{4}$$

The normalized backscatter values are rescaled to 8-bit values based on the global minimum and maximum (Figure 6).

### *2.6. Automated substrate mapping*

Both of the substrate models (Raw and EGN) were trained on non-rectified sonograms. Automated substrate mapping workflows were integrated into PING-Mapper v2.0 (Bodine and Buscombe, 2023a). Once a sonar recording from a Humminbird® has been decoded, substrate classes are predicted from either the raw sonar intensities or EGN sonar intensities, using the respective substrate model, and exported to a zipped Numpy file (npz). The npz stores the model outputs for each substrate class based on the chunk.

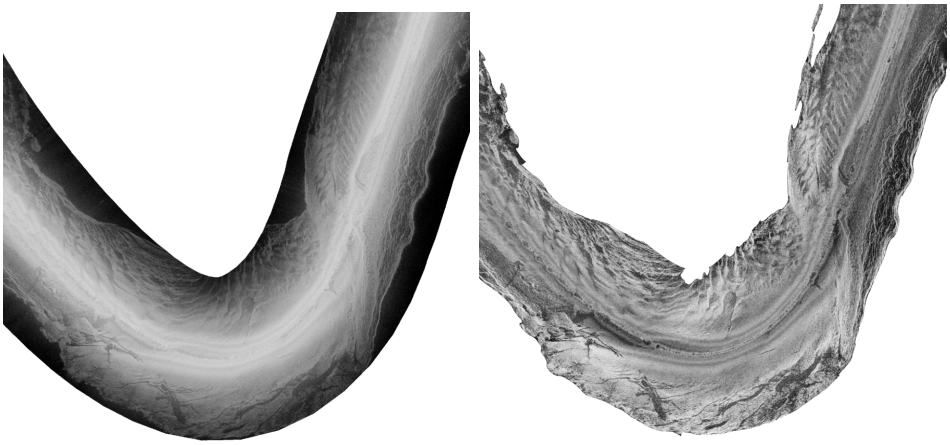

(a) Raw backscatter. (b) EGN backscatter.

Figure 6: Example of georectified mosaics or Raw backscatter (6a) and Empirical Gain Normalized (EGN) backscatter with sonar shadows masked (6b).

For each pixel, the model outputs a vector of real numbers of size $N$ where $N$ is the number of substrate classes. The vector is normalized into a probability distribution of likelihoods [0-1.0] that is proportional to the exponentials of the model outputs using Tensorflow's (Abadi et al., 2015) softmax function. The final classification for a given pixel is the argmax of the likelihood vector. The classification is then georectified into a raster using the same workflows used to georectify sonar mosaics (Bodine et al., 2022), resulting in seamless maps of substrate patches and associated classification (Figure 7). An option for converting the raster substrate map into polygon shapefiles is also provided in PING-Mapper, enabling end-user manual modification of the substrate map in a GIS.

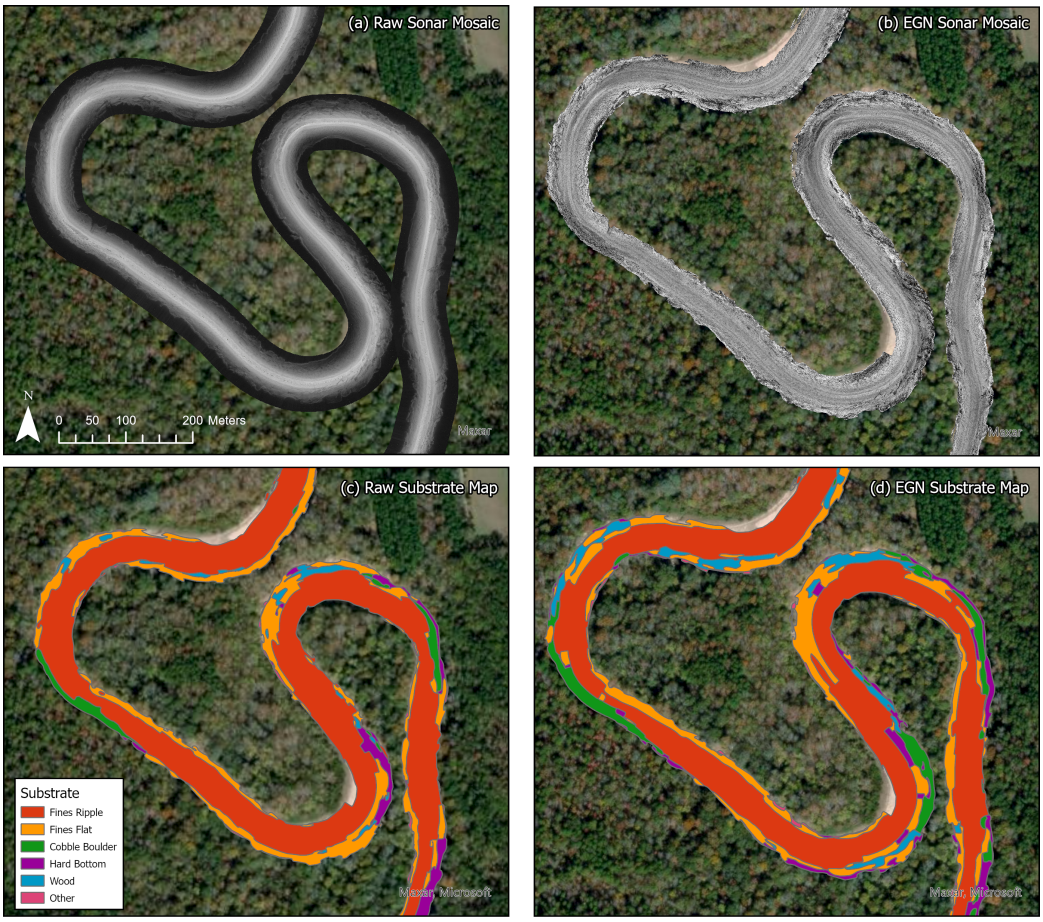


Figure 7: Example of a location on the Chickasawhay River near Waynsboro, MS showing sonar mosaics and mapped substrate predictions produced from the automated workflows in PING-Mapper v2.0. Panel (a) shows the raw sonar mosaic; (b) the EGN sonar mosaic; (c) the substrate map from the raw substrate model; and (d) the map from the EGN substrate model.

## 3. Model evaluation and results

Substrate model evaluation was carried to address two lines of inquiry related to model performance. First, we examine how well the model predictions on hold-out test datasets compare with manually Doodled substrate labels (see Section 2.3.4). Second, we examine how correcting the sonograms with EGN (see Section 2.5) and aligning the existing substrate labels (Section 2.3.4) impacts model performance. Two five-fold cross-validation experiments were used to assess these inquiries with the raw and EGN sonograms. A featureless model, which always predicts the most frequent class in the training dataset (i.e., Rippled Fines or Soft), was included as a baseline for comparison. The data were split such that each sonogram-label pair, of the ∼2,750 pairs, appeared once in one of the five fold's test sets based on the stratified sample of the strataID (see Section 2.4.2). A stratified sample of the remaining sonogram-label pairs was used to assign a pair to the train or validation subsets based on a 40/60 split. Segmentation Gym was again used to generate model-ready datasets (Buscombe and Goldstein, 2022). Only the train subset was augmented to ensure that information from the validation set would not leak into the train set.

Four pixel-wise accuracy metrics are used to evaluate model performance: overall accuracy (OA), mean intersection over union (IoU), frequency-weighted IoU (FwIoU, and Matthews Correlation Coefficient (MCC). OA is the number of correctly predicted pixels, true positive (TP) and true negative (TN) over the total number of pixels. Mean IoU, defined as the average size of the intersection divided by the size of the union between each class label and prediction, is described by $IoU = |Y \cap \widehat{Y}|/|Y| + |\widehat{Y}| - |Y \cap \widehat{Y}|$, where $Y$ is

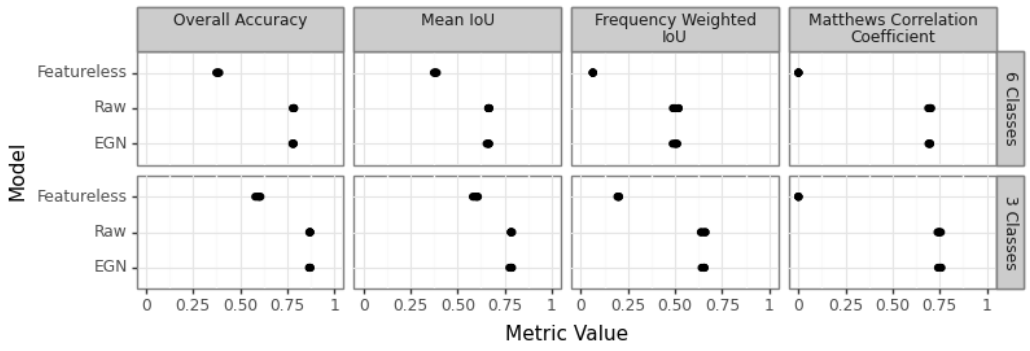


Figure 8: 5-Fold cross validation accuracy metrics for each model (i.e., Featureless, Raw, and EGN). The accuracy metric for each fold of a given model is shown as a point. The top row shows the accuracy metrics for models which predict six classes and the bottom row shows the metrics for predicting three grouped classes.

the label and $\widehat{Y}$ is the prediction. FwIoU accounts for class imbalance by taking the weighted mean based on class frequency. MCC ranges from -1 (perfect prediction-label disagreement) to 1 (perfect prediction-label agreement) where 0 indicates no relationship, and is given by $(TP \times TN - FP \times FN)/(\sqrt{(TP+FP)(TP+FN)(TN+FP)(TN+FN)})$, with TP (true positive), TN (true negative), FP (false positive), and FN (false negative). Figure 8 shows a comparison between models which predict all six substrate classes and models which predict three classes of grouped substrate classes. The remainder of this section describes the results in detail.

Overall accuracy metrics were calculated for the 6 substrate classes for each model's fold, and plotted as a point (Figure 8). Both the Raw and EGN models outperformed a featureless baseline. On average, the featureless model achieved an overall accuracy of 0.38, frequency weighted IoU of 0.38, mean IoU of 0.06, and a Matthews Correlation Coefficient of 0.0. On average,

the overall metrics for both datasets were nearly the same, achieving an overall accuracy of 0.78, frequency weighted IoU of 0.67 and 0.66, Mean IoU of 0.5, and Matthews Correlation Coefficient of 0.7. Accuracy metrics were calculated for the 6 substrate classes from each fold's test dataset and model, and were combined into a confusion matrix for the raw test dataset (Figure 9a) and EGN (Figure 9b) test datasets. Each column represents the labeled (i.e. actual) class and each row is the predicted class. Each column sums to 1.0, where each value along the column indicates the false-negative rate. The diagonal in the confusion matrix represents the proportion of correctly classified pixels, or precision. For the raw dataset, model prediction accuracies ranged from 0.41-0.91 for each of the classes. The most common classes in the dataset received the highest accuracies (Fines - Rippled: 0.91; Hard Bottom: 0.80; Fines - Flat: 0.73). Cobble Boulder had a low accuracy of 0.45 and was most commonly misclassified as Hard Bottom. Wood also had a low accuracy of 0.45 and was most commonly misclassified as Fines Flat. The EGN dataset largely had similar performance as the raw model. It performed worse on Fines - Rippled (0.90) and Fines - Flat (0.71), but did slightly better at predicting Cobble Boulder (0.46), Hard Bottom (0.82), and Wood (0.48).

Combining the six substrate classes into three grouped classes showed improved model metrics for the three models (Figure 8). The Fines - Rippled and Fines - Flat classes were combined into a Soft substrate class, Cobble Boulder and Hard Bottom combined into a Hard substrate class, and Wood and Other were combined into an Other class. On average, both the Raw and EGN datasets achieved overall accuracies of 0.87, mean IoU of 0.65,

and Matthews Correlation Coefficient of 0.75 while the raw dataset had a slightly better frequency weighted IoU of 0.79 compared to 0.78 for the EGN datasets. On average, a featureless model achieved an overall accuracy of 0.59, frequency weighted IoU of 0.59, mean IoU of 0.2, and Matthews Correlation Coefficient of 0.0. This grouping resulted in higher accuracies for each grouped class compared to the underlying subclass (see Figures 10a and 10b).

## 4. Discussion

This study describes an end-to-end framework for processing datasets from recreation-grade sonar instruments, with the following contributions: 1) development of sonogram-label segmentation datasets; 2) training deep learning models; 3) evaluating model performance; and 4) integrating the models in PING-Mapper to enable open-source and reproducible tools for data processing and mapping. This is an improvement over existing manual methods (i.e., Kaeser and Litts (2010)) due to the fact that modeled substrate map generation is efficient and reproducible. Additionally, we encapsulate expert knowledge of substrate identification from sonograms, leveraging a supervised modeling approach, something unsupervised approaches (i.e., Buscombe (2017); Hamill et al. (2018)) do not provide. We demonstrate the value of open-source datasets and models by utilizing transfer learning from pre-trained neural networks, underscoring the importance making workflows, datasets, and models readily available in open-source repositories, enabling future studies to benefit from the contributions of this study.

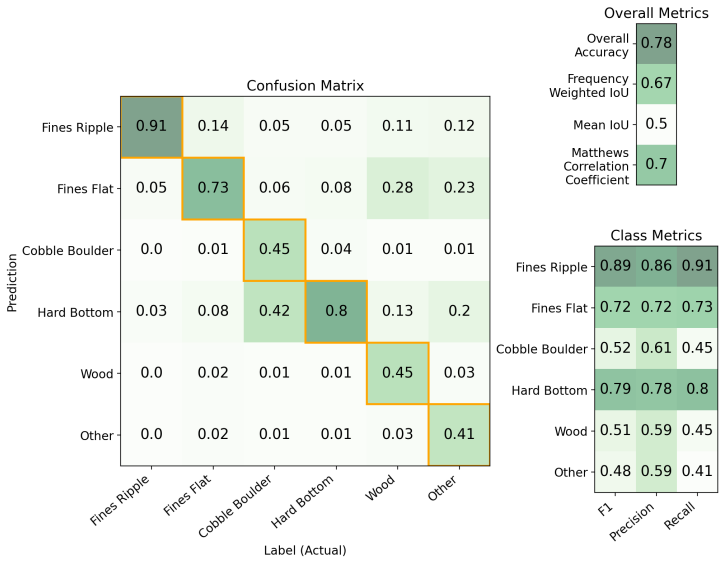


(a) Accuracy metrics for Raw backscatter substrate classification.

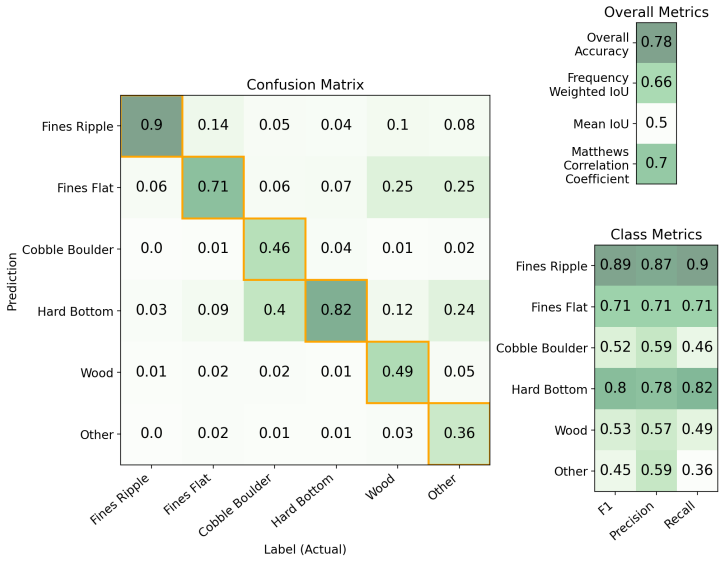


(b) Accuracy metrics for EGN backscatter substrate classification.

Figure 9: 6-class substrate classification accuracy metrics on Raw backscatter (9a) and Empirical Gain Normalized (EGN) backscatter (9b) across all folds.

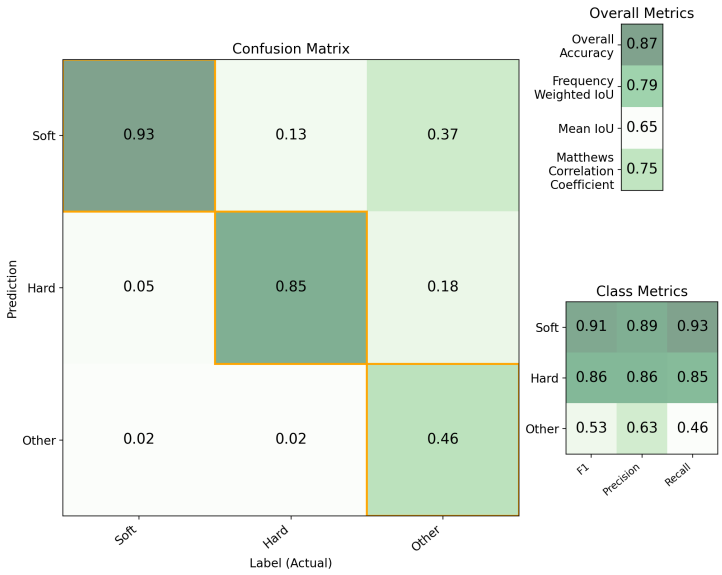


(a) Accuracy metrics for Raw backscatter soft hard, and other classification.

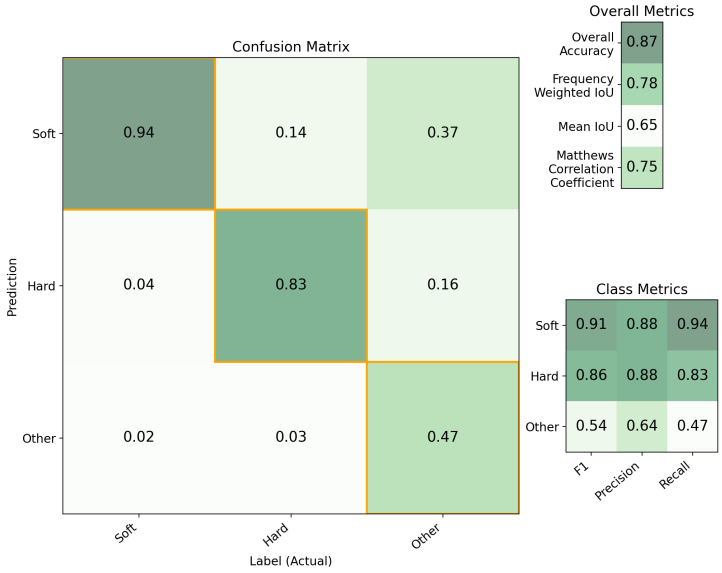


(b) Accuracy metrics for EGN backscatter soft, hard, and other classification.

Figure 10: 3-class substrate classification metrics on Raw backscatter (10a) and EGN backscatter (10b) across all folds. Classes include Soft (fines ripple, fines flat classes), Hard (cobble boulder, hard bottom classes), and Other (all remaining classes).

*4.1. Model output comparison*

The pixel-wise accuracy metrics reported in Figures 9-10 indicate similar performance on each of the substrate classes when comparing the overall accuracies. Examining individual model outputs begin to show where the predictions are in good agreement between each model's prediction and the label, and instances where one of the models outperforms the other. Figure 11a is an example where both model outputs are in strong agreement with one another. They are able to capture the two contiguous patches of hard bottom and delineate the fines that fall between, even though the label misclassified that section as hard bottom (Figure 11a). Agreement between the model outputs does not guarantee that the predictions are accurate, however. Figure 11b shows such a case as both models predicted the hard bottom patch to be fines flat.

There are other instances where one model clearly outperforms the other. The EGN prediction achieves better consensus with the label compared with the raw prediction (Figure 12a). The low contrast and intensity in the hard bottom patch in the Raw image likely contributed to this misclassification while the EGN correction increased the contrast of the rough texture. This does not necessarily make the EGN prediction more accurate in all situations. For example, the Raw predicted hard bottom segmentation in Figure 12b more closely resembles the label. Additionally, the Raw prediction is able segment a larger proportion of the two wood patches while the EGN prediction segments a much smaller area.

When making these comparisons, it is important to consider that all labels were created from Doodling substrates identified from the Raw sonograms.

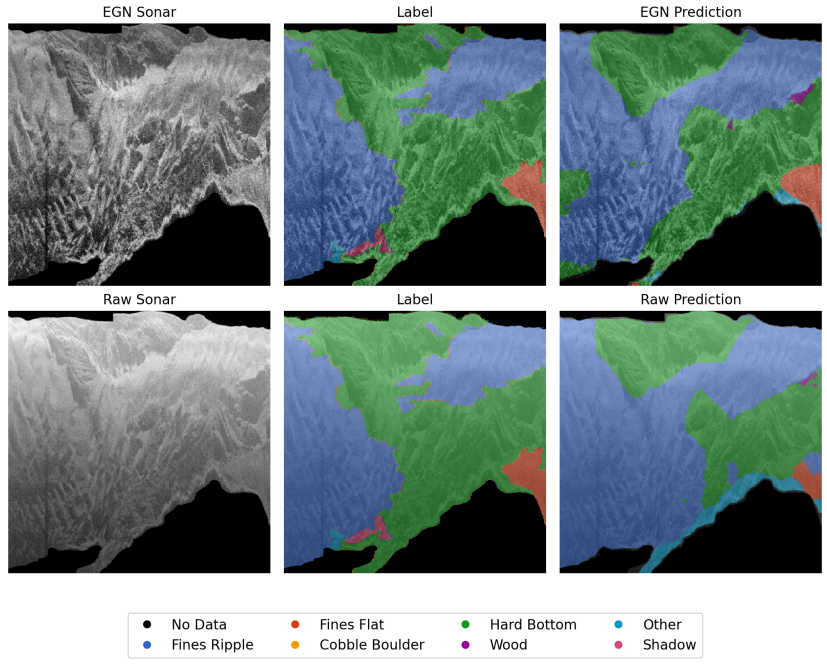


(a) Models correctly classify two distinct hard bottom patches.

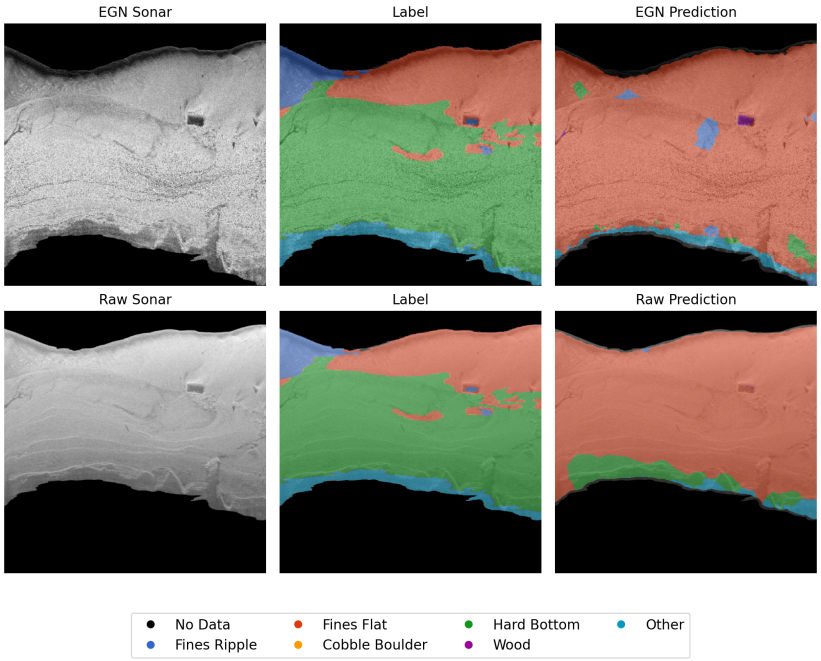


(b) Models both incorrectly classify hard bottom and fines.

Figure 11: Example of agreement between EGN and Raw model outputs.

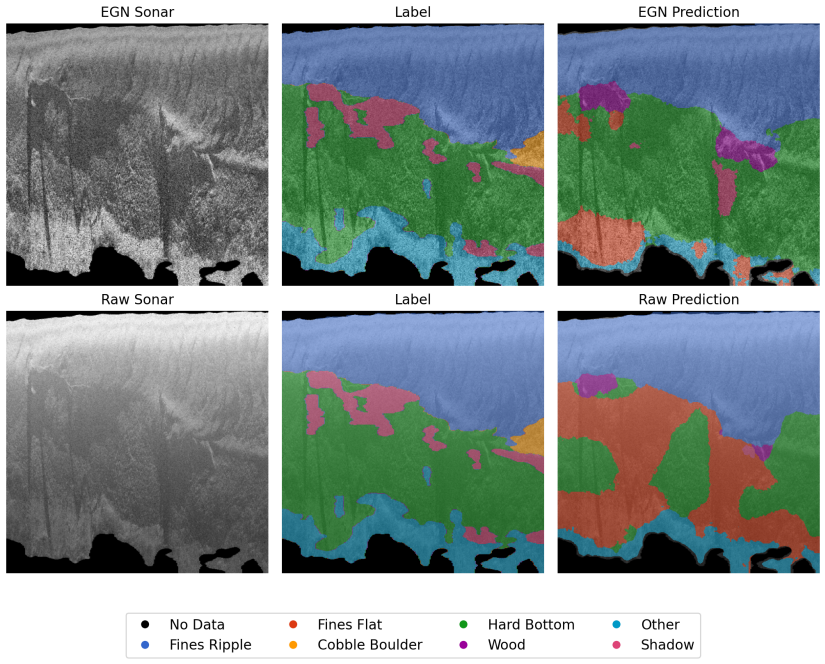


(a) EGN outperforms Raw model.

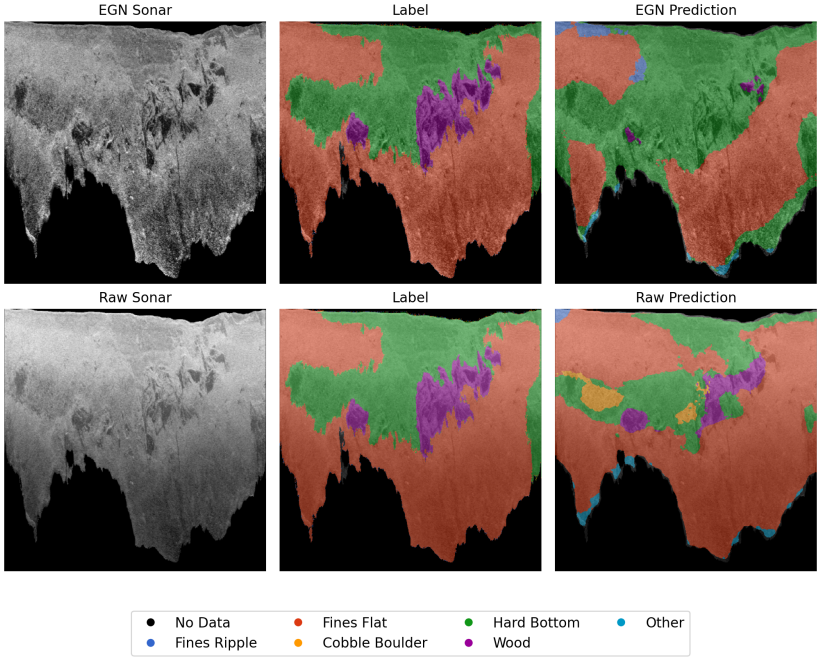


(b) Models both incorrectly classify hard bottom and fines.

Figure 12: Example of disagreement between EGN and Raw model outputs.

The substrate mosaic in Figure 6 and sonograms in Figures 11 and 12 show that EGN corrections increases contrast and brightens low-energy backscatter resulting from sound attenuation. These enhancements would benefit not only the interpretation and Doodling of substrate patches, but may aid fitting of the MLP that Doodler uses for inference to derive pixel-wise labels. Future studies should investigate this further.

### *4.2. Field-based accuracy assessment*

The model metrics reported in this study do not indicate how accurate the maps are compared to true conditions in the field. Future work will assess true map accuracy using reference data collected in the field from these systems, providing an opportunity to compare this automated method with previous manual mapping studies. This accuracy assessment will be less than ideal as 1-3 years will have passed between the scan and field validation. Additionally, the data are collected on highly dynamic alluvial systems that exhibit shifting substrate mosaics which migrate downstream over time. These factors will impact the assessment of true model accuracy and underscores the need for quick, efficient, and reproducible approaches to mapping as presented in this study. These approaches drastically reduce the turn-around time between data collection and mapping from months to hours, providing more opportunity for field assessment, validation, and refining training sets which will ultimately lead to more accurate models and maps.

### *4.3. First open-source sonar image-label datasets*

Evaluating the use of semantic segmentation models on sonar imagery has been limited by the fact that there are no open-source datasets avail-

able, to our knowledge, necessitating the creation of project-specific datasets (Steiniger et al., 2022). As a result, comparisons between existing methods is difficult as there is no common benchmark. Another consideration is that deep neural networks require a large volume of data to train high-quality models, which is expensive with survey-grade sonar systems. In an effort to push the field forward, the depth, shadow, and substrate image-label pairs created for this study are open-source and available for download (Bodine, 2023) to enable future use across studies.

### *4.4. Generalization to other systems*

The sonar data collected for this study, and the models and workflows that result from them, are from datasets collected on highly sinuous Gulf Coastal Plain freshwater river systems in Mississippi (see Figure 2). These rivers contain large proportions of sand and gravel (i.e. fine or soft) substrates with minimal rocky and hardened substrates (Ward et al., 2005). These characteristics are not ubiquitous across all river systems, nor in estuarine and marine environments. Therefore, the applicability and accuracy of these models need to be assessed in the future by studies which utilize these tools and models. If substrate maps generated from these studies are validated and manually revised based on field assessments, they can be shared in an open-source repository, allowing for research in other aquatic systems and further refine model inference. The aquatic community, including researchers, managers, and the public as a whole stands to benefit from sharing their tools, models, and datasets.

## 5. Conclusion

This study has presented a novel approach of automatically mapping substrate patches from recreation-grade side-scan sonar systems using PING-Mapper, an open-source Python package. The first open-source model-ready datasets have been made available which labeled discrete patches of substrate based on expert interpretation and semi-automated delineation using Doodler and Make Sense. An Empirical Gain Normalization (EGN) technique is described and integrated into the package, enabling correction of attenuation to sonar backscatter. The raw and EGN backscatter sonar images along with substrate labels were used to fit two independent semantic segmentation models using prototype-ready workflows in Segmentation Gym. The resulting models were integrated in PING-Mapper, enabling efficient and reproducible export of georefrenced substrate maps. The substrate models achieved an overall accuracy of 78%. This method greatly improves substrate map generation across the landscape by removing the need to manually delineate and classify substrates from recreation-grade side-scan sonar instruments.

## 6. Data Availability

PING-Mapper software (Version 2.0.0) (Bodine and Buscombe, 2023a) developed for this manuscript is licensed under MIT and archived on Zenodo (`https://doi.org/10.5281/zenodo.10120054`). All training datasets (Bodine, 2023) and segmentation models (Bodine and Buscombe, 2023b) are licensed under MIT and archived on Zenodo (`https://doi.org/10.5281/zenodo.10119320`; `https://doi.org/10.5281/zenodo.10093642`). The lat-

est version of PING-Mapper is published on GitHub (`https://github.com/CameronBodine/PINGMapper`).

## 7. Acknowledgments

This study was made possible by a partnership between the U.S. Fish and Wildlife Service (USFWS) and Northern Arizona University (NAU). Funding for this work was provided by the Open Ocean Trustee Implementation Group to restore natural resources injured by the 2010 Deepwater Horizon oil spill in the Gulf of Mexico. The findings and conclusions in this article are those of the authors and do not necessarily represent the views of the U.S. Fish and Wildlife Service. Thanks to Mike Andres of the University of Southern Mississippi (USM), Eric Haffey (USM), Kasea Price (USM), Katherine Wright (USM), Adam Kaeser (USFWS), and Channing St. Aubin (USFWS) for data collection and planning, and to Adam Kaeser (USFWS) and Jennylyn Redner (AZGFD) for helpful comments. C. Bodine acknowledges support from USFWS [F19AC00836].

## References

Abadi, M., Agarwal, A., Barham, P., Brevdo, E., Chen, Z., Citro, C., Corrado, G.S., Davis, A., Dean, J., Devin, M., Ghemawat, S., Goodfellow, I., Harp, A., Irving, G., Isard, M., Jia, Y., Jozefowicz, R., Kaiser, L., Kudlur, M., Levenberg, J., Mané, D., Monga, R., Moore, S., Murray, D., Olah, C., Schuster, M., Shlens, J., Steiner, B., Sutskever, I., Talwar, K., Tucker, P., Vanhoucke, V., Vasudevan, V., Viégas, F., Vinyals, O.,

Warden, P., Wattenberg, M., Wicke, M., Yu, Y., Zheng, X., 2015. TensorFlow: Large-Scale Machine Learning on Heterogeneous Systems. URL: https://www.tensorflow.org/.

Bennett, D.L., Bister, T.J., Ott, R.A., 2020. Using Recreation-Grade Side-Scan Sonar to Produce Classified Maps of Submerged Aquatic Vegetation. North American Journal of Fisheries Management 40, 145–153. doi:10.1002/nafm.10386.

Bishop, C.M., 2006. Pattern Recognition and Machine Learning. Springer.

Blondel, P., 2009. The Handbook of Sidescan Sonar. Springer Berlin Heidelberg, Berlin, Heidelberg. doi:10.1007/978-3-540-49886-5.

Bodine, C.S., 2023. Sidescan Sonar Substrate, Depth, and Shadow Image-Label-Pairs (v1.0.0) [Data set]. doi:10.5281/zenodo.10119320.

Bodine, C.S., Buscombe, D., 2022. PING-Mapper (v1.0.0) [Software]. doi:10.5281/zenodo.6604785.

Bodine, C.S., Buscombe, D., 2023a. PING-Mapper (v2.0.0) [Software]. doi:10.5281/zenodo.10120054.

Bodine, C.S., Buscombe, D., 2023b. Sidescan Sonar Substrate, Depth, and Shadow Models for PINGMapper v2.0.0 (v1.0.2) [Model]. doi:10.5281/zenodo.10093642.

Bodine, C.S., Buscombe, D., Best, R.J., Redner, J.A., Kaeser, A.J., 2022. PING-Mapper: Open-Source Software for Automated Benthic Imaging

and Mapping Using Recreation-Grade Sonar. Earth and Space Science 9. doi:10.1029/2022EA002469.

Bollinger, M.A., Kline, R.J., 2017. Validating Sidescan Sonar as a Fish Survey Tool over Artificial Reefs. Journal of Coastal Research 336, 1397–1407. doi:10.2112/JCOASTRES-D-16-00174.1.

Brennan, S.R., Torgersen, C.E., Hollenbeck, J.P., Fernandez, D.P., Jensen, C.K., Schindler, D.E., 2016. Dendritic network models: Improving isoscapes and quantifying influence of landscape and in-stream processes on strontium isotopes in rivers. Geophysical Research Letters 43, 5043–5051. doi:10.1002/2016GL068904.

Brown, C.J., Smith, S.J., Lawton, P., Anderson, J.T., 2011. Benthic habitat mapping: A review of progress towards improved understanding of the spatial ecology of the seafloor using acoustic techniques. Estuarine, Coastal and Shelf Science 92, 502–520. doi:10.1016/j.ecss.2011.02.007.

Buscombe, D., 2017. Shallow water benthic imaging and substrate characterization using recreational-grade sidescan-sonar. Environmental Modelling & Software 89, 1–18. doi:10.1016/j.envsoft.2016.12.003.

Buscombe, D., Goldstein, E.B., 2022. A Reproducible and Reusable Pipeline for Segmentation of Geoscientific Imagery. Earth and Space Science 9. doi:10.1029/2022EA002332.

Buscombe, D., Goldstein, E.B., Sherwood, C.R., Bodine, C., Brown, J.A., Favela, J., Fitzpatrick, S., Kranenburg, C.J., Over, J.R., Ritchie, A.C., Warrick, J.A., Wernette, P., 2022. Human-in-the-Loop Segmentation

of Earth Surface Imagery. Earth and Space Science 9, e2021EA002085. doi:10.1029/2021EA002085.

Buscombe, D., Grams, P.E., Smith, S.M.C., 2016. Automated Riverbed Sediment Classification Using Low-Cost Sidescan Sonar. Journal of Hydraulic Engineering 142, 06015019. doi:10.1061/(ASCE)HY.1943-7900.0001079.

Carbonneau, P., Fonstad, M.A., Marcus, W.A., Dugdale, S.J., 2012. Making riverscapes real. Geomorphology 137, 74–86. doi:10.1016/j.geomorph.2010.09.030.

Carbonneau, P.E., Bizzi, S., 2023. Global mapping of river sediment bars. Earth Surface Processes and Landforms doi:10.1002/esp.5739.

Cheek, B.D., Grabowski, T.B., Bean, P.T., Groeschel, J.R., Magnelia, S.J., 2016. Evaluating habitat associations of a fish assemblage at multiple spatial scales in a minimally disturbed stream using low-cost remote sensing. Aquatic Conservation: Marine and Freshwater Ecosystems 26, 20–34. doi:10.1002/aqc.2569.

Chesapeake Technology Inc., 2023. Empirical Gain Normalization (EGN). URL: https://chesapeaketech.com/wp-content/uploads/docs/SonarWiz7_UG/HTML/index.htm.

Chesterman, W.D., Clynick, P.R., Stride, A.H., 1958. An acoustic aid to sea bed survey. Acta Acustica united with Acustica 8.

Cobra, D., Oppenheim, A., Jaffe, J., 1992. Geometric distortions in side-scan sonar images: a procedure for their estimation and correction. IEEE Journal of Oceanic Engineering 17, 252–268. doi:10.1109/48.153442.

Drozdzal, M., Vorontsov, E., Chartrand, G., Kadoury, S., Pal, C., 2016. The Importance of Skip Connections in Biomedical Image Segmentation, Springer International Publishing, Cham, pp. 179–187. doi:10.1007/978-3-319-46976-8_19.

Hamill, D., Buscombe, D., Wheaton, J.M., 2018. Alluvial substrate mapping by automated texture segmentation of recreational-grade side scan sonar imagery. PLOS ONE 13, e0194373. doi:10.1371/journal.pone.0194373.

Holcomb, K.M., Schueller, P., Jelks, H.L., Knight, J.R., Allen, M.S., 2020. Use of Strong Habitat–Abundance Relationships in Assessing Population Status of Cryptic Fishes: An Example Using the Harlequin Darter. Transactions of the American Fisheries Society 149, 320–334. doi:10.1002/tafs.10231.

Kaeser, A.J., Litts, T.L., 2008. An Assessment of Deadhead Logs and Large Woody Debris Using Side Scan Sonar and Field Surveys in Streams of Southwest Georgia. Fisheries 33, 589–597. doi:10.1577/1548-8446-33.12.589.

Kaeser, A.J., Litts, T.L., 2010. A Novel Technique for Mapping Habitat in Navigable Streams Using Low-cost Side Scan Sonar. Fisheries 35, 163–174. doi:10.1577/1548-8446-35.4.163.

Kaeser, A.J., Litts, T.L., Tracy, T.W., 2013. Using Low-Cost Side-Scan Sonar for Benthic Mapping Throughout the Lower Flint River, Georgia, USA. River Research and Applications 29, 634–644. doi:10.1002/rra.2556.

Kaeser, A.J., Smit, R., Gangloff, M., 2019. Mapping and Modeling the Distribution, Abundance, and Habitat Associations of the Endangered Fat Threeridge in the Apalachicola River System. Journal of Fish and Wildlife Management 10, 653–675. doi:10.3996/032019-JFWM-021.

Klein, M., Edgerton, H., 1968. Sonar- a modern technique for ocean exploitation. IEEE Spectrum 5, 40–46. URL: http://ieeexplore.ieee.org/document/5214684/, doi:10.1109/MSPEC.1968.5214684.

Kubat, M., 2017. An Introduction to Machine Learning. Springer International Publishing. doi:10.1007/978-3-319-63913-0.

Kumar, S., Hebert, M., 2006. Discriminative Random Fields. International Journal of Computer Vision 68, 179–201. doi:10.1007/s11263-006-7007-9.

Lawson, K.M., Ridgway, J.L., Mueller, A.T., Faulkner, J.D.A., Calfee, R.D., 2020. Semiautomated Process for Enumeration of Fishes from Recreational-Grade Side-Scan Sonar Imagery. North American Journal of Fisheries Management 40, 75–83. doi:10.1002/nafm.10373.

Li, K., Yu, F., Wang, Q., Wu, M., Li, G., Yan, T., He, B., 2019. Real-Time Segmentation of Side Scan Sonar Imagery for AUVs, in: 2019 IEEE Underwater Technology (UT), IEEE. pp. 1–5. doi:10.1109/UT.2019.8734319.

Liu, C.C., Zhang, Y.C., Chen, P.Y., Lai, C.C., Chen, Y.H., Cheng, J.H., Ko, M.H., 2019. Clouds Classification from Sentinel-2 Imagery with Deep Residual Learning and Semantic Image Segmentation. Remote Sensing 11, 119. doi:10.3390/rs11020119.

Murphy, K.P., 2012. Machine Learning: A Probabilistic Perspective. The MIT Press.

Myrvold, K.M., Kind Dervo, B., 2020. Flight elevation and water clarity affect the utility of unmanned aerial vehicles in mapping stream substratum. Fisheries Management and Ecology 27, 167–169. doi:10.1111/fme.12394.

Nagi, A.S., Kumar, D., Sola, D., Scott, K.A., 2021. RUF: Effective Sea Ice Floe Segmentation Using End-to-End RES-UNET-CRF with Dual Loss. Remote Sensing 13, 2460. doi:10.3390/rs13132460.

Nian, R., Zang, L., Geng, X., Yu, F., Ren, S., He, B., Li, X., 2021. Towards Characterizing and Developing Formation and Migration Cues in Seafloor Sand Waves on Topology, Morphology, Evolution from High-Resolution Mapping via Side-Scan Sonar in Autonomous Underwater Vehicles. Sensors 21, 3283. doi:10.3390/s21093283.

Niu, S., Liu, Y., Wang, J., Song, H., 2020. A Decade Survey of Transfer Learning (2010–2020). IEEE Transactions on Artificial Intelligence 1, 151–166. doi:10.1109/TAI.2021.3054609.

Peterson, E.E., Ver Hoef, J.M., Isaak, D.J., Falke, J.A., Fortin, M.J., Jordan, C.E., McNyset, K., Monestiez, P., Ruesch, A.S., Sengupta, A., Som, N., Steel, E.A., Theobald, D.M., Torgersen, C.E., Wenger, S.J., 2013. Modelling dendritic ecological networks in space: an integrated network perspective. Ecology Letters 16, 707–719. doi:10.1111/ele.12084.

Rahnemoonfar, M., Dobbs, D., 2019. Semantic Segmentation of Underwater Sonar Imagery with Deep Learning, in: IGARSS 2019 - 2019 IEEE Interna-

tional Geoscience and Remote Sensing Symposium, IEEE. pp. 9455–9458. doi:10.1109/IGARSS.2019.8898742.

Ronneberger, O., Fischer, P., Brox, T., 2015. U-Net: Convolutional Networks for Biomedical Image Segmentation, Springer International Publishing, Cham, pp. 234–241. doi:10.1007/978-3-319-24574-4_28.

Scholl, E., Cross, W., Baxter, C., Guy, C., 2021. Uncovering process domains in large rivers: Patterns and potential drivers of benthic substrate heterogeneity in two North American riverscapes. Geomorphology 375, 107524. doi:10.1016/j.geomorph.2020.107524.

Singh, H., Adams, J., Mindell, D., Foley, B., 2000. Imaging Underwater for Archaeology. Journal of Field Archaeology 27, 319–328. doi:10.1179/jfa.2000.27.3.319.

Skalski, P., 2019. Make Sense [Software]. URL: https://github.com/SkalskiP/make-sense/.

Smit, R., Kaeser, A., 2016. Defining freshwater mussel mesohabitat associations in an alluvial, Coastal Plain river. Freshwater Science 35, 1276–1290. doi:10.1086/688928.

Song, Y., He, B., Liu, P., 2021. Real-Time Object Detection for AUVs Using Self-Cascaded Convolutional Neural Networks. IEEE Journal of Oceanic Engineering 46, 56–67. doi:10.1109/JOE.2019.2950974.

Steiniger, Y., Kraus, D., Meisen, T., 2022. Survey on deep learning based computer vision for sonar imagery. Engineering Applications of Artificial Intelligence 114, 105157. doi:10.1016/j.engappai.2022.105157.

Torgersen, C.E., Le Pichon, C., Fullerton, A.H., Dugdale, S.J., Duda, J.J., Giovannini, F., Tales, É., Belliard, J., Branco, P., Bergeron, N.E., Roy, M.L., Tonolla, D., Lamouroux, N., Capra, H., Baxter, C.V., 2022. Riverscape approaches in practice: perspectives and applications. Biological Reviews 97, 481–504. doi:10.1111/brv.12810.

Walker, D.J., Alford, J.B., 2016. Mapping Lake Sturgeon Spawning Habitat in the Upper Tennessee River using Side-Scan Sonar. North American Journal of Fisheries Management 36, 1097–1105. doi:10.1080/02755947.2016.1198289.

Wang, H., Gao, N., Xiao, Y., Tang, Y., 2020. Image feature extraction based on improved FCN for UUV side-scan sonar. Marine Geophysical Research 41, 18. doi:10.1007/s11001-020-09417-7.

Ward, G.M., Harris, P.M., Ward, A.K., 2005. Gulf Coast Rivers of the Southeastern United States, in: Rivers of North America. Elsevier, pp. 124–178. doi:10.1016/B978-012088253-3/50007-9.

Wolfenkoehler, W., Long, J.M., Gary, R., Snow, R.A., Schooley, J.D., Bruckerhoff, L.A., Lonsinger, R.C., 2023. Viability of side-scan sonar to enumerate Paddlefish, a large pelagic freshwater fish, in rivers and reservoirs. Fisheries Research 261, 106639. doi:10.1016/j.fishres.2023.106639.

Wu, Wang, Rigall, Li, Zhu, He, Yan, 2019. ECNet: Efficient Convolutional Networks for Side Scan Sonar Image Segmentation. Sensors 19, 2009. doi:10.3390/s19092009.

Xie, E., Wang, W., Yu, Z., Anandkumar, A., Alvarez, J.M., Luo, P., 2021. SegFormer: Simple and Efficient Design for Semantic Segmentation with Transformers, in: Ranzato, M., Beygelzimer, A., Dauphin, Y., Liang, P.S., Vaughan, J.W. (Eds.), Advances in Neural Information Processing Systems, Curran Associates, Inc.. pp. 12077–12090. URL: https://proceedings.neurips.cc/paper_files/paper/2021/file/64f1f27bf1b4ec22924fd0acb550c235-Paper.pdf.

Yu, F., Zhu, Y., Wang, Q., Li, K., Wu, M., Li, G., Yan, T., He, B., 2019. Segmentation of Side Scan Sonar Images on AUV, in: 2019 IEEE Underwater Technology (UT), IEEE. pp. 1–4. doi:10.1109/UT.2019.8734433.

Zhang, Z., Liu, Q., Wang, Y., 2018. Road Extraction by Deep Residual U-Net. IEEE Geoscience and Remote Sensing Letters 15, 749–753. doi:10.1109/LGRS.2018.2802944.

Zheng, G., Zhang, H., Li, Y., Zhao, J., 2021. A Universal Automatic Bottom Tracking Method of Side Scan Sonar Data Based on Semantic Segmentation. Remote Sensing 13, 1945. doi:10.3390/rs13101945.

Zhou, B., Zhao, H., Puig, X., Xiao, T., Fidler, S., Barriuso, A., Torralba, A., 2019. Semantic Understanding of Scenes Through the ADE20K Dataset. International Journal of Computer Vision 127, 302–321. doi:10.1007/s11263-018-1140-0.